Improvement of Hydraulic Characteristics for Impellers Using the Finite Volume Analysis

Maryna Demianenko, Oleksandr Starynskyi, Bohdan Vashyst, Ivan Pavlenko, Oleksandr Liaposhchenko, and Vitalii Ivanov

1 Introduction

One of the most crucial pump cards is the head–capacity curve, which is the dependence between the pump head and the volumetric flow. The shape of this card depends on the pump type, its design features, and other parameters. There are two types of the head–capacity curve: theoretical and experimental. The theoretical one is determined by applying the fundamental equations of hydrodynamics with the corresponding assumptions and simplifications; the experimental one is based on experimental data. Both have the following disadvantages: for the first—it accurately reflects only the qualitative relationship between the main parameters; for the second—it is resource-intensive. One of the main problems of the pump operation process is cavitation (gas bubbles formation process due to a sharp pressure change caused by the fast increase of the fluid velocity). The above process is characterized by the cavitation number, defined as:

$$\mathrm{Ca} = \frac{p - p_v}{\frac{1}{2}\rho U^2}, \tag{1}$$

where p—flow pressure, p_v—vapor pressure, $\frac{1}{2}\rho U^2$—dynamic pressure.

The primary way for cavitation avoidance is to minimize the underpressure value in the critical areas, which can partially be achieved by increasing the ambient pressure. In particular, the main thing for the cavitation preventing is to ensure

M. Demianenko · O. Starynskyi · B. Vashyst · I. Pavlenko · O. Liaposhchenko · V. Ivanov (✉)
Sumy State University, Sumy, Ukraine
e-mail: ivanov@tmvi.sumdu.edu.ua

D. Cagáňová et al. (eds.), *Advances in Industrial Internet of Things, Engineering and Management*, EAI/Springer Innovations in Communication and Computing,
https://doi.org/10.1007/978-3-030-69705-1_10

suction pressure, which provides the overcoming fluid flow without hydraulic losses in the suction line and the suction chamber. The inducer can be used for the above purpose.

Typically, cavitation is considered separately from the phase–temperature transition due to its processing speed, which leads to the assumption of thermal equilibrium unacceptably. The mass transfer is determined by a purely mechanical interaction (the pressure difference at the liquid–vapor interface) and not dependent on thermal interaction in the simplest cavitation model. Currently, many types of research are aimed at models that consider both effects.

2 Literature Review

The reliability of hydraulic motors is a topical engineering problem. A specific design method was proposed to increase reliability based on the developed mathematical tools through simulating changes in a technical state of the rotors in a hydraulic motor [1]. The study [2] introduces the design schemes, a mathematical tool, and a calculation algorithm that were developed to justify the angular arrangement of the moving distributor. In the research study [3], a design model, a mathematical apparatus, and a calculation algorithm were developed to solve the problem of manufacturing workability improvement. The reliability of pneumatic and hydraulic machines is very acute. Experimental studies on a specially designed experimental setup with a supercharger model proved that the ejection ratio for the solid particle is twice that of the jet ejectors [4]. The experimental studies proved the possibility of improvement of cavitation erosion characteristics in the centrifugal inducer stage with the inducer bush [5]. Due to the rapid development of modern computer technology, nowadays, many computer programs based on the finite volume method are used for simulation hydrodynamics in multiple channels. Modeling viscous flow hydrodynamics using state-of-the-art software products is widely used by leading foreign researchers to solve pump engineering problems [6–13]. Engineering calculations are complicated and time-consuming tasks, so they should be automated and integrated with computer-aided systems. It can ensure the implementation of the Industry 4.0 strategy [14–16]. The right and the correct choice of the turbulence and cavitation models was made by the consideration of a number of the scientific works of this direction. One of the most widely used software is ANSYS CFX [17–19], which allows you to study the fluid flow in the pump and obtain the head–capacity curve. It should be noted that the head–capacity curve obtained from numerical simulation has a good correlation with experimental results subject to a provided computational model. So, it can be used for the optimization of the introduced geometry before pump production. The parametric method for constructing geometry is necessary. The Design Modeler unit, in particular, Blade Modeler [20], is used for profiling blades. ANSYS Blade Modeler is a powerful specialized tool for working with the geometry of machine blades; it allows you to create parametric models of the blade ring using both the available theoretical

drawings and the CAD model. The integrated design modules allow creating the geometry of a centrifugal machine from scratch with the subsequent construction of a parametric three-dimensional geometry model for analysis and optimization.

The calculation of the fluid flow is carried out by numerically solving a system of equations describing the most general case of fluid motion—the Navier–Stokes equations and the continuity equation. The Reynolds equations are used with the closure by the turbulence models in ANSYS CFX—the widely used SST turbulence model. According to this model, the system of equations of fluid motion is supplemented by two differential equations describing the transfer, respectively, of the kinetic energy of turbulence k and the dissipation rate ε (for the main flow) and ω (for boundary layer).

$$\frac{\partial}{\partial t}(\rho k) + \frac{\partial}{\partial x_j}\left(\rho \overline{u_j} k\right) = \frac{\partial}{\partial x_j}\left(\Gamma_k \frac{\partial k}{\partial x_j}\right) + P_k - \rho\varepsilon, \tag{2}$$

$$\frac{\partial}{\partial t}(\rho\varepsilon) + \frac{\partial}{\partial x_j}\left(\rho \overline{u_j} \varepsilon\right) = \frac{\partial}{\partial x_j}\left(\Gamma_\varepsilon \frac{\partial \varepsilon}{\partial x_j}\right) + \frac{\varepsilon}{k}\left(C_{\varepsilon 1} P_k - \rho C_{\varepsilon 2}\varepsilon\right), \tag{3}$$

where $P_k = -\rho\overline{u_i' u_j'}\frac{\partial \overline{u_i}}{\partial x_j}$—energy expression term k.

The cavitation process in the flow part of the centrifugal stages is considering using a combination of the Reilly–Plessis model implemented to the multiphase flow and interphase mass transfer model. A uniform multiphase model is usually used for flows with cavitation.

The Reilly–Plessis equation is the basis for the equation determining the rate of formation of steam and condensate; it describes the growth of gas bulbs in a liquid, defined as:

$$R_\mathrm{B}\frac{a^2 R_\mathrm{B}}{dt^2} + \frac{3}{2}\left(\frac{d R_\mathrm{B}}{dt}\right)^2 + \frac{2\sigma}{\rho_\mathrm{f} R_\mathrm{B}} = \frac{p_v - p}{\rho_\mathrm{f}}, \tag{4}$$

where R_B—bubble radius, p_v—bubble pressure, p—fluid pressure around the bubble, ρ_f—fluid density, σ—surface tension coefficient between liquid and vapor.

Given the above, the main aim of this paper is to construct the parametric geometry of the elements centrifugal pump and determine the main operation parameters by using the finite volume method.

3 Research Methodology

The main elements creation of the pump centrifugal stage, namely the impeller, the booster, the inducer, and the inlet distribution part, was carried out using the Blade Modeler software package (Fig. 1).

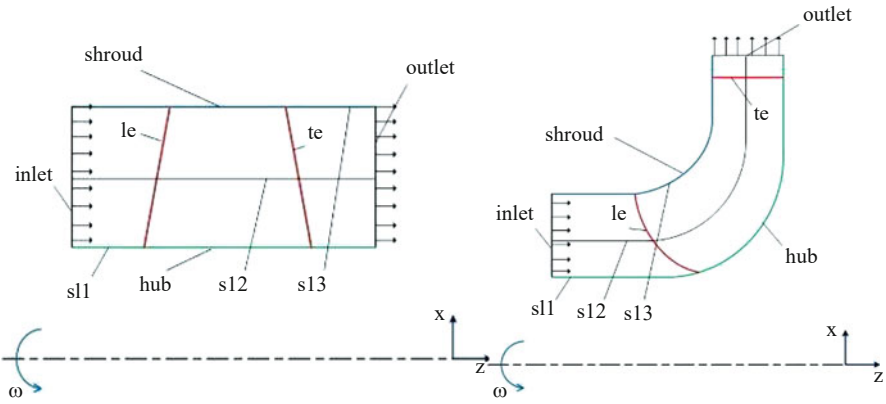

Fig. 1 The geometry designing elements in the Blade Modeler software

Table 1 The geometry designing elements in the Blade Modeler software

Inlet	Inlet part
Outlet	Outlet part
Hub	Internal streamline
Shroud	Outer streamline
le	Entrance edge of the blade
te	Exit edge of the blade
sl	Streamline

The model designing of the interlobe space using the Blade Modeler has certain specifics. The parametric geometry designing using the Blade Modeler is implemented using the seven elements shown in Table 1.

The interlobe space model of almost any blades configuration may be generated using these seven elements. It should be noted that the above elements are designing in a meridional projection.

By default, the impeller's rotation is carried out only *OZ*-axis around, the positive direction of the working fluid flow coincides with the *OZ*-axis direction, the positive direction of rotation of the flowing part is clockwise, viewed from the working area entrance side.

At the first stage of the geometry designing the primary elements sketches (inlet, outlet, hub, shroud) was created. The dimension lines and their sizes were assigned for each of the elements that were specified, which allows changing them if it is necessary. Figure 2 shows the resulting interlobe space contours.

The second stage was the interlobe space generation and blades generation using the FlowPath and Blade tool, respectively. In addition to the meridional projection configuration, the blades are also characterized by angles, namely the wrap angles (φ) and blade installation angles at the inlet and outlet edges (βb). The Blade Modeler provides blades profiling in two modes: the wrap angles and the angle

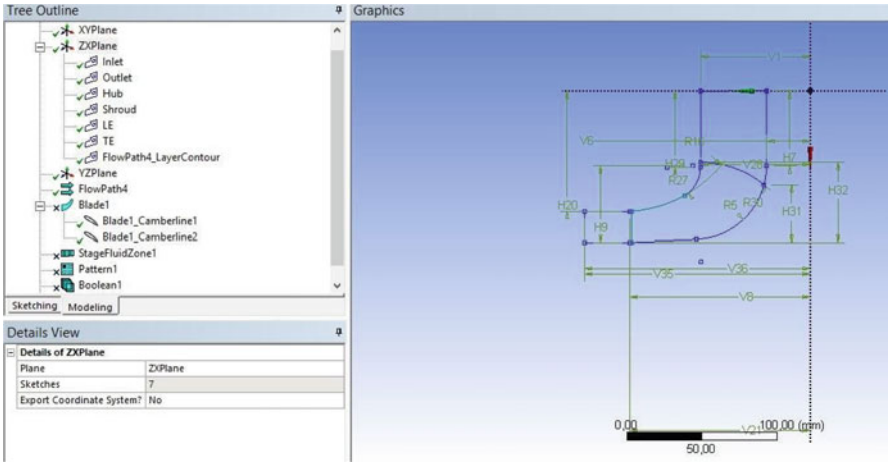

Fig. 2 The interlobe space contours

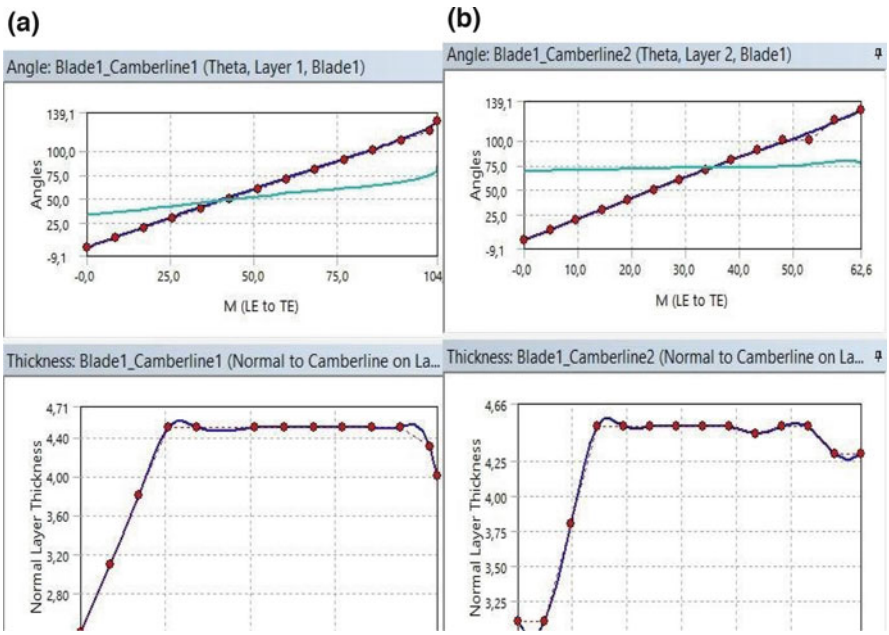

Fig. 3 Blade_Camberline: (**a**) internal streamline; (**b**) outer streamline

of installation, and these parameters are interconnected. The value changing of one parameter in a certain way changes the second parameter value. Blade profiling was performed using Blade_Camberline. It should be noted that for profiling the blades along the internal streamline (hub) along the streamline (SL) and the outer streamline (shroud), there are individual Blade_Camberline. Figure 3 shows

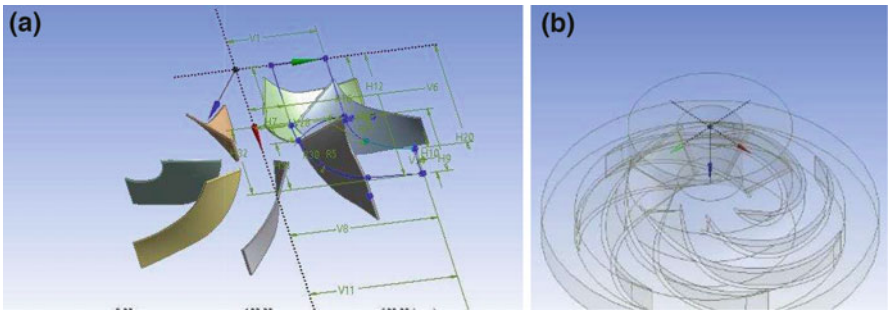

Fig. 4 Impeller blades (**a**) and interlobe space (**b**)

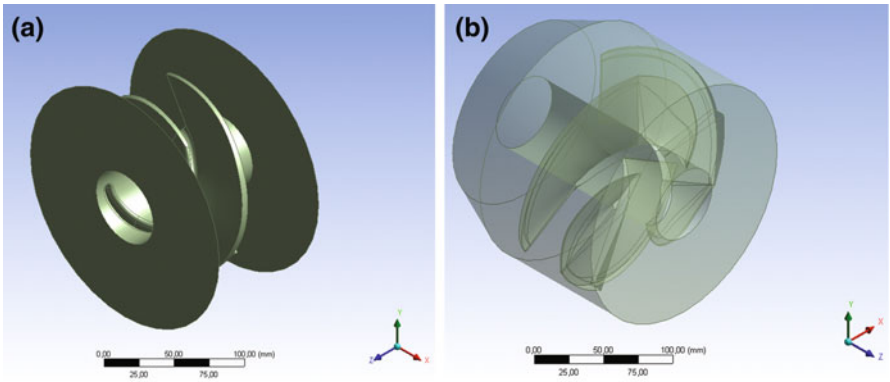

Fig. 5 Booster (**a**) and inducer (**b**)

Blade_Camberline for an internal streamline and an outer streamline. As a profiling result, the blade configurations, shown in Fig. 4, were obtained. The last stage is to blades thickness imparts, which was also done using Blade_Camberline. The booster geometry and inducer geometry were generated in the same way. As a parametric geometry designing result, the three-dimensional models of the impeller, the booster, and the inducer, shown in Figs. 4 and 5, were generated.

The rectilinear region of the 3D model with a flow distributor is shown in Fig. 6.

After creating 3D models, the mesh for all parts of the centrifugal stage was developed using the ANSYS Meshing mesh generator (Fig. 7). The booster mesh and the inducer mesh are presented in Figs. 8 and 9, respectively.

The mesh was generated for each flow part separately, after which they were combined in the CFX pre-processor into one in the following sequence: the rectilinear region, then the booster, the inducer, and the impeller (Fig. 10). In the single-phase flow simulation with non-cavitation as the boundary conditions at the

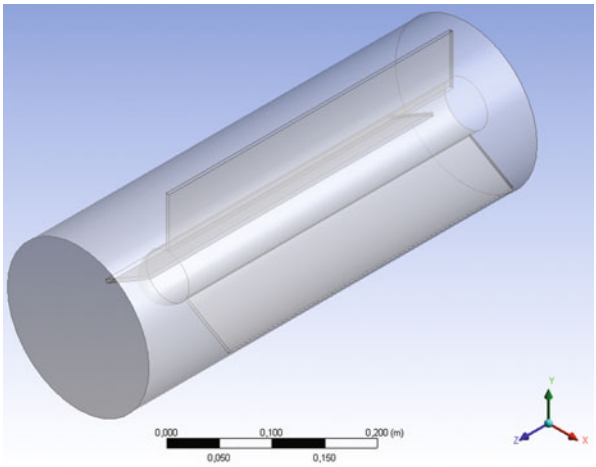

Fig. 6 The rectilinear region of the 3D model with a flow distributor

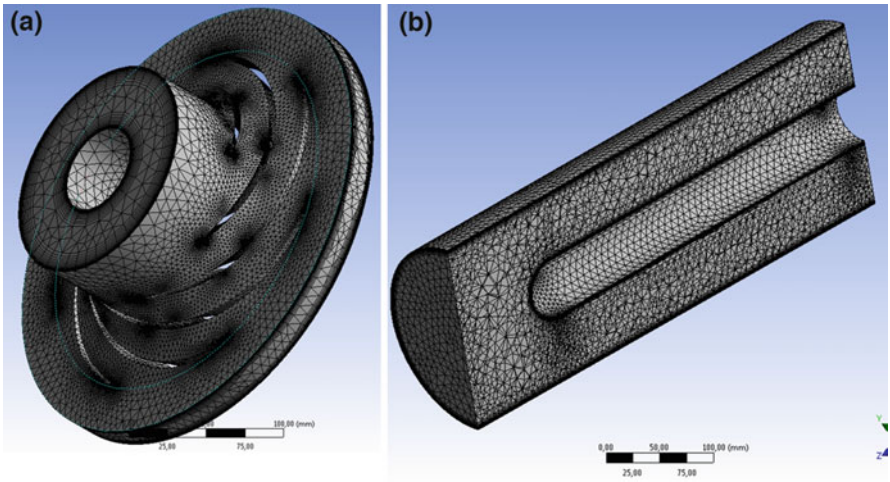

Fig. 7 The impeller mesh with 2.9×10^6 cells (**a**) and the rectilinear region mesh (**b**)

computational domain inlet was set mass flow rate, at the computational domain outlet—static pressure equals 1 MPa. The boundary condition type was configured as "opening" since it was assumed that backflows at the computational domain exit existed.

For all computational domain walls, the velocity which is equal to zero (the "sticking" condition) was specified. The walls were roughness; the mean arithmetic deviation of the profile (R_a) was 6.3 μm. The interface areas of the interaction verges of the rotor and stator elements were determined. The interface type was specified as a "frozen rotor", which assumed parameter averaging at time. The input parameters are shown in Table 2.

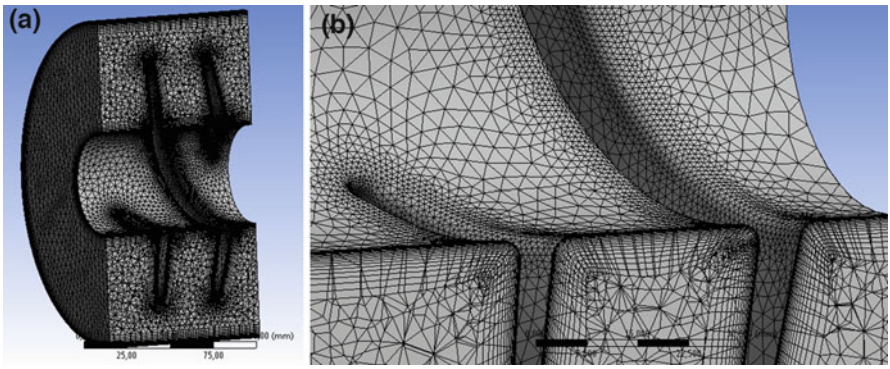

Fig. 8 The booster mesh with 1.7×10^6 cells

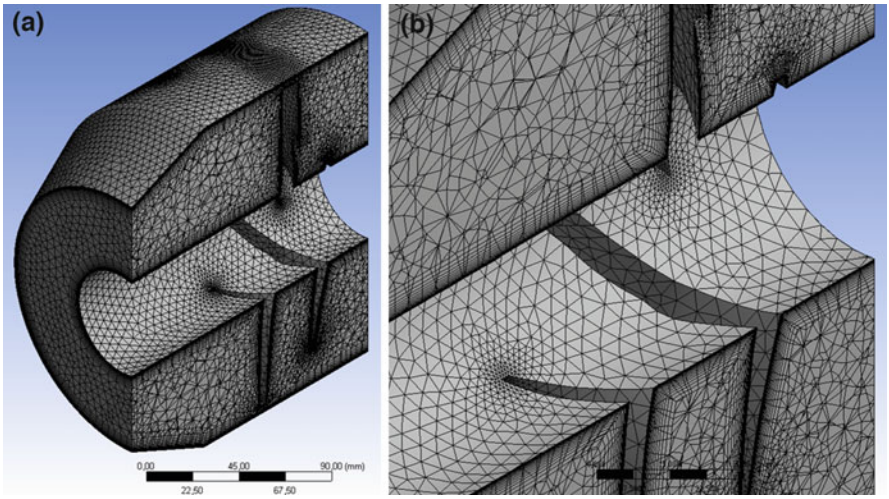

Fig. 9 The inducer mesh with 1.6×10^6 cells

4 Results

The values of velocity and pressure in the calculated areas were obtained as a result of a numerical simulation. Figures 11 and 12 show the pressure fields on the surfaces of a centrifugal impeller, a booster, and an inducer.

The presence of zones with reduced pressure can be noted after consideration of the total pressure contours (Figs. 11 and 12). These are the zones of the most probable occurrence of cavitation cavities. Figures 13 and 14 show velocity vectors in the entire computational domain and separately around the booster and inducer.

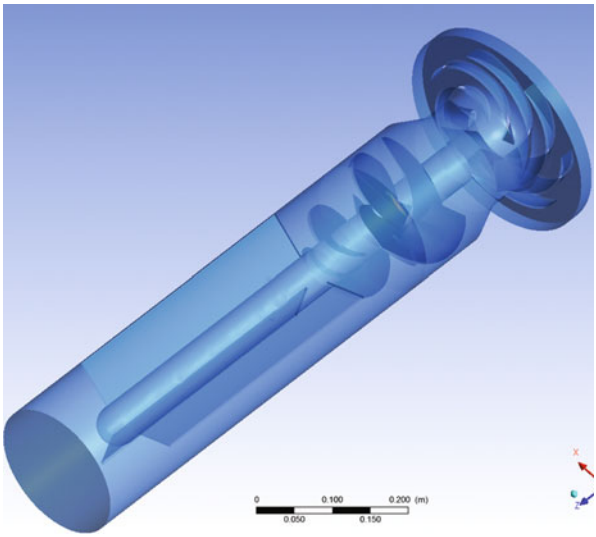

Fig. 10 The centrifugal stage flow part

Table 2 Input parameter for the flow hydrodynamics modeling in the centrifugal stage

Rotation frequency, n	2940 rpm
Density, ρ	997 ks/m^3
Saturated pressure at $t = 25$ °C	3196 pa
Barometric pressure	101,325 pa

The main aim of the flow study in a centrifugal pump is the analysis of the flow structure at the outlet from the inducer. The dimensionless values of the flow parameters were used for the analysis. Meridian component of absolute velocity:

$$\overline{V}_{\mathrm{m}} = \frac{V_{\mathrm{m}}}{\left(\overline{V}_{\mathrm{mcp}}\right)_G}. \tag{5}$$

Circumferential component of velocity:

$$\overline{\upsilon}_u = \frac{\upsilon_u}{u_{\mathrm{pc}}}. \tag{6}$$

where u_{pc}—the circumferential velocity at the outer diameter.

Figures 15, 16 and 17 show the velocity fields distribution at the outlets of the booster and inducer and pressure field.

The pump head and flow, as well as the power and efficiency, were determined as a result of the calculation. The pressure of the centrifugal stage was calculated as the ratio of the pressure difference at the outlet and the inlet of the flow density to

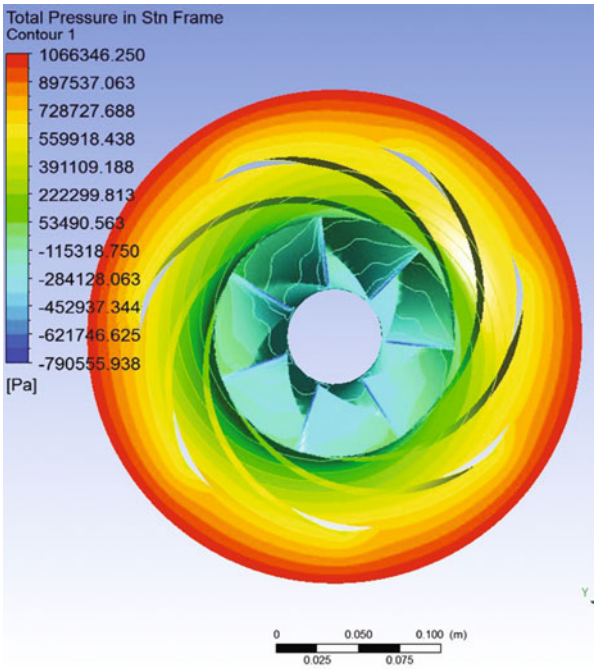

Fig. 11 The distribution of the total pressure on the surface of the centrifugal impeller

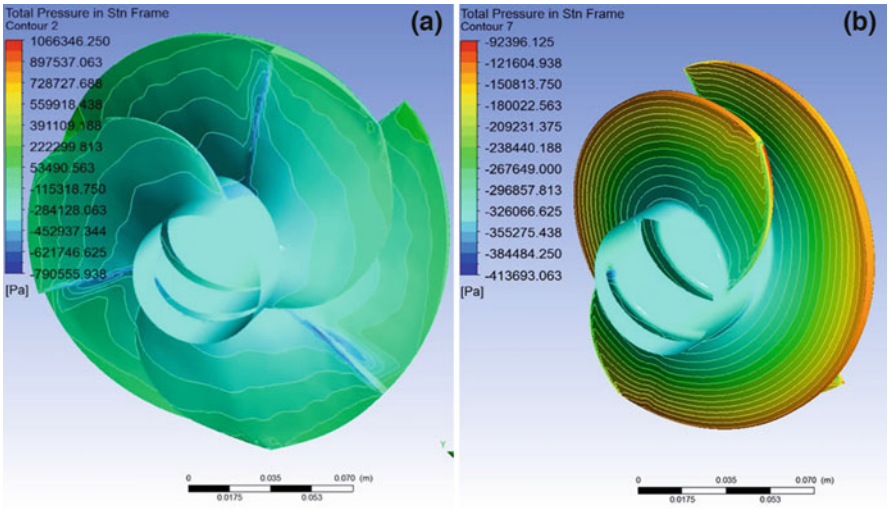

Fig. 12 The distribution of the total pressure on the surface of the inducer (**a**) and the booster's surface (**b**)

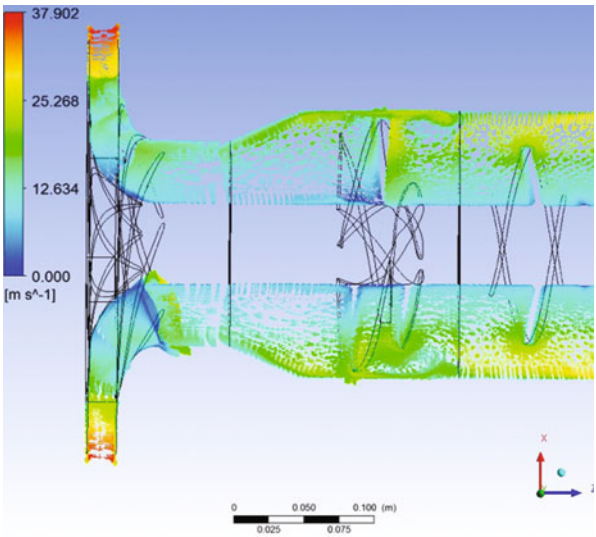

Fig. 13 Velocity vectors in the computational domain

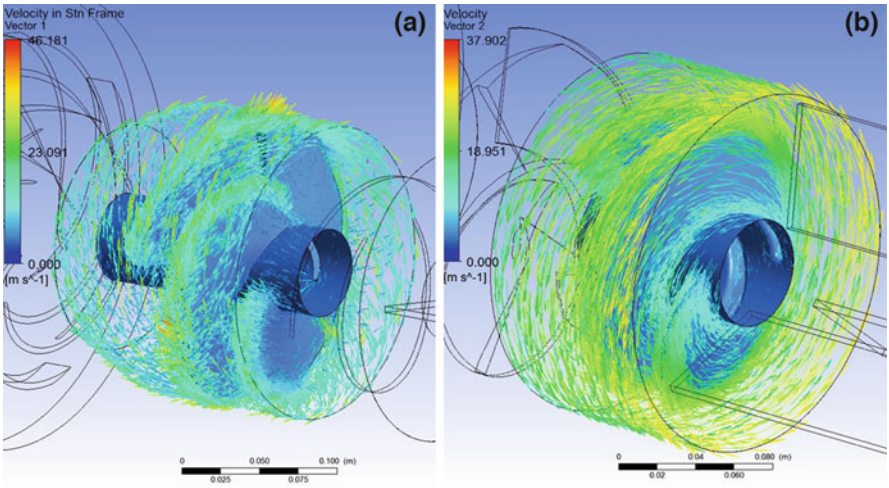

Fig. 14 Velocity vectors around the inducer (**a**) and the booster (**b**)

the acceleration of gravity and amounted to $H = 43.6$ m. The feed of the centrifugal stage is equal to $Q = 236.5$ m^3/s. The pump power was determined by the torque and amounted to $N = 2.86 \times 10^4$ W at a frequency of 2940 rpm. By the following dependence, the pump efficiency was calculated ($\eta = 0.98$):

$$\eta = \frac{\rho g Q H}{3.6 \times 10^3 \cdot N}. \tag{7}$$

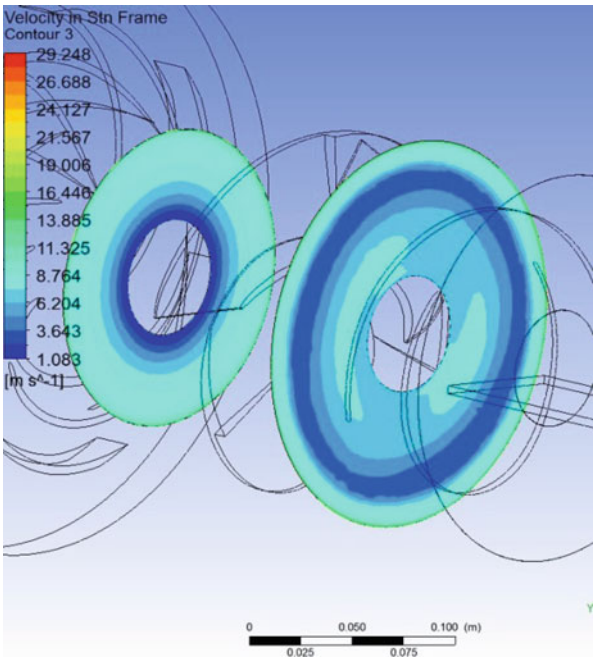

Fig. 15 Velocity distribution at the outlet of the inducer and booster

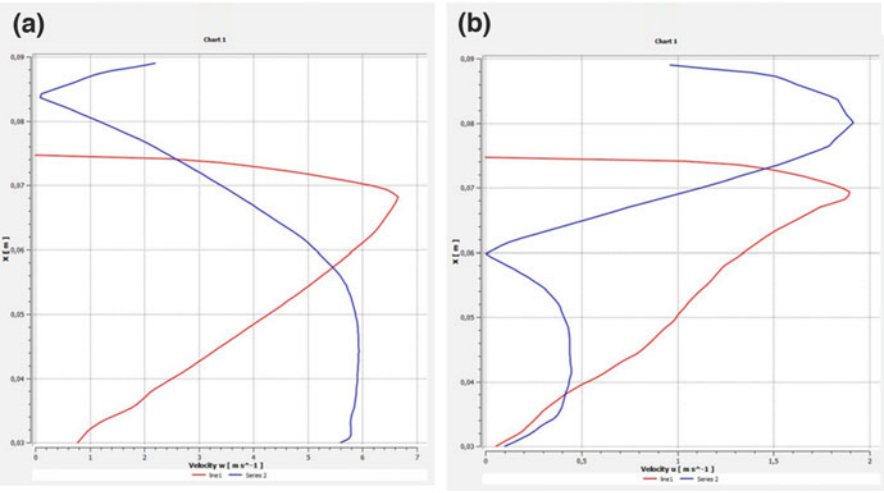

Fig. 16 Distribution graph of the meridian (w) velocity component (**a**) and circumferential (u) component of velocity (**b**) at the outlet of the inducer

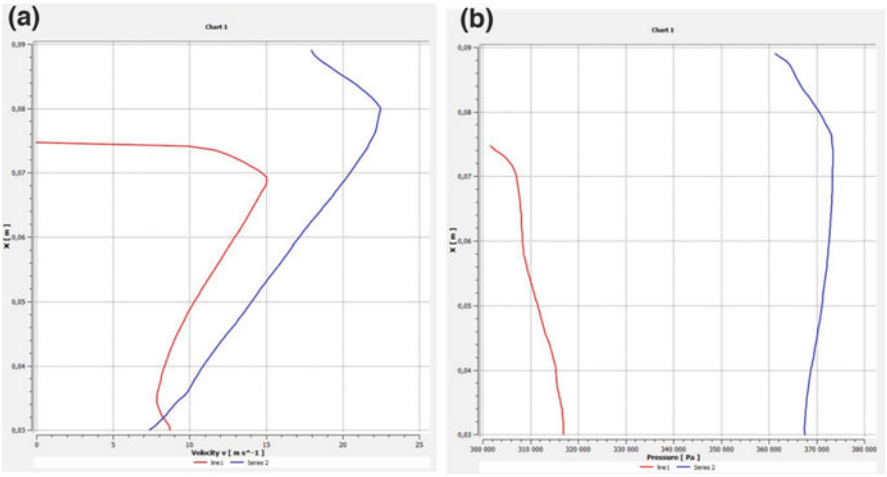

Fig. 17 Distribution graph of the radial (v) velocity component (**a**) and pressure (P) at the outlet of the booster (**b**)

5 Conclusions

The parametrized geometry of the centrifugal stage main elements, namely the impeller, the booster, and the inducer, was done using the Blade Modeler module of the ANSYS software package, for the blades profiling, and given them thickness the Blade_Camberline tool was used. A flow hydrodynamics simulation in the centrifugal stage using the finite volume method was carried out. Based on the simulation results, the individual element's local characteristics of the centrifugal stage were determined, namely the pressure difference on the blade's surface, the flow speed directions of the inducer interlobe space, and the booster inducer. The meridional, axial, and radial velocity components of the inducer are also determined. The centrifugal stage main characteristics, namely the head ($H = 43.6$ m) and the flow rate ($Q = 236.5$ m^3/s), the power ($N = 2.86 \times 10^4$ W) and efficiency ($\eta = 0.98$), was determined. It was noted that the simultaneous use of an inducer and booster reduces pressure drops and, as a result, cavitation.

Acknowledgments This research is partially funded by Center for Industrial Engineering (Sumy State University), International Association for Technological Development and Innovations, and research grants No. 0117U003931 and No. 0120U102036 (Ministry of Education and Science of Ukraine).

References

1. A. Panchenko, A. Voloshina, I. Panchenko, O. Titova, A. Pastushenko, Reliability design of rotors for orbital hydraulic motors. IOP Conf. Ser. Mater. Sci. Eng. **708**(1), 012017 (2019). https://doi.org/10.1088/1757-899X/708/1/012017

2. A. Voloshina, A. Panchenko, I. Panchenko, O. Titova, A. Zasiadko, Improving the Output Characteristics of Planetary Hydraulic Machines. IOP Conf. Ser. Mater. Sci. Eng. **708**(1), 012038 (2019). https://doi.org/10.1088/1757-899X/708/1/012038
3. A. Voloshina, A. Panchenko, O. Boltyansky, O. Titova, Improvement of manufacture workability for distribution systems of planetary hydraulic machines, in *Advances in Design, Simulation and Manufacturing II. DSMIE 2019*, Lecture Notes in Mechanical Engineering, ed. by V. Ivanov et al., (Springer, Cham, 2020), pp. 732–741. https://doi.org/10.1007/978-3-030-22365-6_73
4. A. Rogovyi, Energy performances of the vortex chamber supercharger. Energy **163**, 52–60 (2018). https://doi.org/10.1016/j.energy.2018.08.075
5. P. Tkach, A. Yashchenko, O. Gusak, S. Khovanskyy, V. Panchenko, I. Grechka, Improvement of cavitation erosion characteristics of the centrifugal inducer stage with the inducer bush. Eastern-Eur. J. Enterp. Technol. **4**(8–94), 24–31 (2018). https://doi.org/10.15587/1729-4061.2018.139392
6. F. Shi, H. Tsukamoto, Numerical study of pressure fluctuations caused by impeller-diffuser interaction in a diffuser pump stage. J. Fluids Eng. **123**(3), 466–474 (2001)
7. W. Ma et al., Experimental observation of a generalized thouless pump with a single spin. Phys. Rev. Lett. **120**(12), 120501 (2018)
8. H. Wang, H. Tsukamoto, Fundamental analysis on rotor-Stator interaction in a diffuser pump by vortex method. J. Fluids Eng. **123**(4), 737–747 (2001)
9. J. Sun, H. Tsukamoto, Off-design performance prediction for diffuser pumps. Proc. Inst. Mech. Eng. A J. Power Energy **215**(2), 191–201 (2001)
10. H. Tsukamoto, H. Ohashi, Transient characteristics of a centrifugal pump during starting period. J. Fluids Eng. **104**(1), 6–13 (1982)
11. W. Qin, H. Tsukamoto, Theoretical study of pressure fluctuations downstream of a diffuser pump impeller—part 1: Fundamental analysis on rotor-Stator interaction. J. Fluids Eng. **119**(3), 647–652 (1997)
12. S.-M. Kwon, H.S. Kang, J.-H. Shin, Rotor profile design in a hypogerotor pump. J. Mech. Sci. Technol. **23**(12), 3459–3470 (2009)
13. H.J. Kong, S.J. Kang, K.S. Yun, H.J. Lim, An experimental study on the cooling and heating performance of a residential ground source heat pump system. Korean J. Air-Cond. Refrig. Eng. **25**(3), 156–163 (2013)
14. S. Saniuk, A. Saniuk, D. Cagáňová, Cyber industry networks as an environment of the Industry 4.0 implementation. Wirel. Netw. (2019). https://doi.org/10.1007/s11276-019-02079-3
15. N. Horňáková, L. Jurík, H. Hrablik Chovanová, D. Cagáňová, D. Babčanová, AHP method application in selection of appropriate material handling equipment in selected industrial enterprise. Wirel. Netw. (2019). https://doi.org/10.1007/s11276-019-02050-2
16. V. Švač, D. Cagáňová, Managerial skills for innovation support. Mobile. Netw. Appl. (2020). https://doi.org/10.1007/s11036-020-01517-3
17. P. Dupont, E. Casartelli, Numerical prediction of the cavitation in pumps, in *Symposia and General Papers, Parts A and B*, vol. 2 (2002)
18. R. Ferman et al., Boiler feed pump rerate for increased head and reduced cavitation, in *3rd ASME Pumping Machinery Symposium*, Vancouver, Canada (1997)
19. J.P. Franc, The Rayleigh-Plesset equation: A simple and powerful tool to understand various aspects of cavitation, in *Fluid Dynamics of Cavitation and Cavitating Turbopumps*, CISM International Centre for Mechanical Sciences, ed. by L. d'Agostino, M. V. Salvetti, vol. 496, (Springer, Vienna, 2007)
20. L. Shabliy, A. Cherniaev, Optimization of gas turbine compressor blade parameters for gas-dynamic efficiency under strength constraints, in *Proceedings of the 4th International Conference on Simulation and Modeling Methodologies, Technologies and Applications* (2014)